Rotational-Flows for Interpolation Between Sampled Surfaces

Joshua H. Levy, Mark Foskey, and Stephen M. Pizer
University of North Carolina at Chapel Hill
levy@cs.unc.edu

Abstract

We introduce a shape-maintaining method for interpolating between sampled surfaces. This method works sample by sample and requires correspondence between the reference and target surfaces' samples, which henceforth we call vertices. This method is based on the assumption that a frame for orientation is available at each vertex. In the plane, each oriented vertex moves locally along a circular arc as if it were rotating to its destination. The generalization of this interpolation to three dimensions causes each oriented vertex to move along a helical path that combines in-plane rotation with translation along the axis of rotation.

We show that the planar flows provide shape-maintaining interpolations when the reference and target objects are similar. Moreover, the interpolations are size maintaining when the reference and target objects are congruent. In three dimensions, similarity transformations are interpolated by an affine transformation that generally preserves shape better than the alternative of interpolating vertices along linear paths irrespective of changes in orientation. In both two and three dimensions we have experimental evidence that when non-shape-preserving deformations are applied to template shapes, the interpolation tends to be visually satisfying with each intermediate object appearing to belong to the same class of objects as the end points. We have extended this method to interpolate medially represented shape models of anatomical objects in 3D.

1. Introduction

There are many interesting applications for surface interpolation. Perhaps the most direct application is to generate animations to visualize the differences between objects. In the general realm of shape analysis, a surface interpolation scheme can be used to measure the difference between objects which in turn can be used to align objects or calculate a mean. In the more specialized field of medical image analysis the paths that boundary points follow during the interpolation can be used to drive a registration process which then enables morphometry and atlas-based segmentation. It is these latter problems, registration and atlas-based segmentation, that have inspired this research.

The graphics community has been interested in creating visually pleasing morphs between objects. For example, the work by Breen and Whitaker [2] can be used to interpolate between implicitly represented shapes. The implicit shape representation allows for changes in topology. Although this feature is valued in the context of general purpose animation, in our target applications it is undesirable.

Recent work by Vaillant and Glaunes [11] and by Glaunes and Joshi [5] has used the concept of currents from differential geometry to define a metric on shapes. This metric is then used to drive an optimization that produces a diffeomorphic warp under the large deformation framework [8]. This warp can then be used to bring the reference shape forward, through a series of interpolating shapes, and into its target configuration. However, the computation needed to produce this warp can be expensive.

Pizer *et al*. [10] advocate the use of medial shape representations (m-reps) because of their ability to describe nonlinear shape changes such as bending, twisting, and widening. Fletcher *et al*. [4] showed that each medial atom in an m-rep object lies on a manifold, and that geodesics on this manifold can be defined using a standard Riemannian metric [3]. A pair of m-rep objects can be interpolated by interpolating each pair of corresponding medial atoms along the geodesic between them. However, as a medial atom follows such a geodesic, it moves along a linear path in $\mathbb{R}^3$ independent of the changes to its orientation and size. Due to the straight-line nature of these paths, a pair of medial atoms could collide during the interpolation, creating an undesired fold in the image space. Even if no atoms collide during the interpolation, an interpolated surface may not appear to belong to the intended object class.

In this work we propose a novel interpolation that uses orientation information to move the vertices along curved paths. The path for each vertex is computed from information that is local to that vertex. These paths are easy to compute and easy to understand. Although our method is not guaranteed to produce a diffeomorphism, it does tend to produce visually satisfying interpolations that under certain

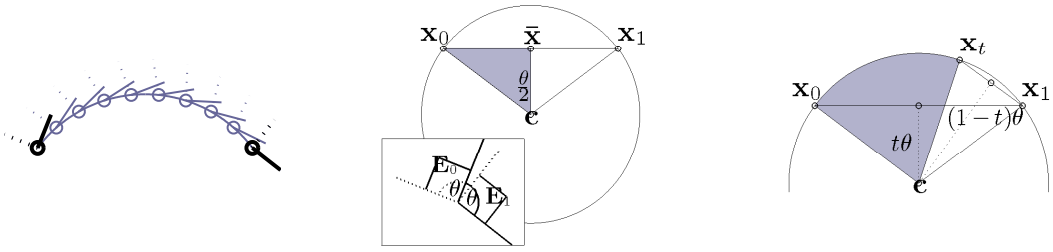

Figure 1. (Left) Examples of planar points: $\mathbf{x}_0$ and $\mathbf{x}_1$ and the corresponding frames: $\mathbf{E}_0$ and $\mathbf{E}_1$. The solid line indicates the $\mathbf{e}_{0,t}$ basis direction, and the dotted line indicates $\mathbf{e}_{1,t}$. The interpolation provided by our method is indicated by a lighter color. Note that the frame rotates concurrently with the point. (Center) The geometry of rotational-flows interpolation in two dimensions. The rotation required to bring $\mathbf{E}_0$ onto $\mathbf{E}_1$ (inset) defines the angle θ swept out by the interpolating path from $\mathbf{x}_0$ to $\mathbf{x}_1$. The path lies on a circle whose geometry can be derived from the positions of the points and the angle θ. (Right) The point $\mathbf{x}_t$ is reached after interpolating t fraction of the way from $\mathbf{x}_0$ to $\mathbf{x}_1$. If we then interpolate from $\mathbf{x}_t$ to $\mathbf{x}_1$ out method continues along the original circular arc.

circumstances have shape-preserving properties.

We describe our methods for interpolating point-normal pairs in a plane, point-frame pairs in three dimensions, and m-rep shape models in Section 2. We show interpolations produced by our method on synthetic data in two and three dimensions, and on m-rep models of a lung during the respiratory cycle in Section 3. We conclude with a summary of these results and a discussion of future work.

2. Methods

Throughout this paper we will use the following notation. Let $\mathbf{x} = (x, y) \in \mathbb{R}^2$ denote a point in the plane. Let $\mathbf{E} = \{\mathbf{e_1}, \mathbf{e_2}\} \in \mathbf{SO}(2)$ denote an orthogonal basis for a frame in two dimensions. The reference curve, $S[0] = \{(\mathbf{x}_{i,0}, \mathbf{E}_{i,0})\}$ is a discrete set of points, indexed by i, with each oriented by its frame. The target curve, $S[1]$ is defined similarly, and a correspondence is assumed between $(\mathbf{x}_{i,0}, \mathbf{E}_{i,0})$ and $(\mathbf{x}_{i,1}, \mathbf{E}_{i,1})$. A similar definition applies in three dimensions, with $\mathbf{x} \in \mathbb{R}^3$ and $\mathbf{E} \in \mathbf{SO}(3)$ discrete samples of a surface.

The rotational-flows interpolation for a set of oriented points indexed by i in $N \in \{2, 3\}$ dimensions will define a set of functions $f_i : (0, 1) \rightarrow \mathbb{R}^N \times \mathbf{SO}(N)$ with the property that $f_i(0) = (\mathbf{x}_{i,0}, \mathbf{E}_{i,0})$, $f_i(1) = (\mathbf{x}_{i,1}, \mathbf{E}_{i,1})$, and $f_i(t)$ smoothly interpolates along the time axis t.

As a convention, we will discuss a single function f which interpolates between point-frame pairs $(\mathbf{x}_0, \mathbf{E}_0)$ and $(\mathbf{x}_1, \mathbf{E}_1)$. The full interpolation is given by applying the set of f_i to the corresponding data.

2.1. Interpolation in two dimensions

Our method interpolates between a pair of oriented points by sweeping out a circular arc between $\mathbf{x}_0$ and $\mathbf{x}_1$ that covers an angle equal to the angular distance between the frames $\mathbf{E}_0$ and $\mathbf{E}_1$. An example of such an interpolation can be seen in the left pane of Fig. 1.

Let $\bar{\mathbf{x}} = \frac{1}{2}(\mathbf{x}_0 + \mathbf{x}_1)$, $\Delta\mathbf{x} = \mathbf{x}_1 - \mathbf{x}_0$, and $\mathbf{x}_\perp$ be a unit vector in the direction found by rotating $\Delta\mathbf{x}$ counterclockwise by 90 degrees. The geometry of the circular path defined by our method is illustrated in the center pane of Fig. 1. The center $\mathbf{c}$ is equidistant to $\mathbf{x}_0$ and $\mathbf{x}_1$, so it must lie on their perpendicular bisector: the line $\bar{\mathbf{x}} + \alpha\mathbf{x}_\perp$ for some parameter α. The angle $\theta \in (-\pi, \pi]$ is defined as the angle between $\mathbf{e}_{0,0}$ and $\mathbf{e}_{0,1}$ with a positive sign indicating counterclockwise rotation. Our method identifies a center of rotation, $\mathbf{c}$ such that the angle subtended by $\mathbf{x}_0, \mathbf{c}$, and $\mathbf{x}_1$ is θ. From the geometry in Fig. 1, it follows that

$$\mathbf{c} = \bar{\mathbf{x}} + \frac{\cos\frac{\theta}{2}\|\Delta\mathbf{x}\|}{2\sin\frac{\theta}{2}}\mathbf{x}_\perp \quad (1)$$

$$f(t) = (\mathbf{c} + \mathbf{R}_{t\theta}(\mathbf{x}_0 - \mathbf{c}), \mathbf{R}_{t\theta}\mathbf{E}_0) \quad (2)$$

where $\mathbf{R}_{t\theta}$ denotes rotation by $t\theta$ degrees.

The denominator in (1) is 0 when $\theta = 0$. We use the limiting behavior to define the interpolation in this case. When $\theta = 0$, $\mathbf{E}_0 = \mathbf{E}_1$, so it is natural to think of $f(t)$ as not having a rotational component. If we consider $\lim_{\theta\rightarrow 0}$ (1) then $\mathbf{c}$ is infinitely far from the data points, and the circular arc connecting them is a straight line.

$$\lim_{\theta\rightarrow 0} f(t) = (\mathbf{x}_0 + t(\mathbf{x}_1 - \mathbf{x}_0), \mathbf{E}), \quad (3)$$

where $\mathbf{E} = \mathbf{E}_0 = \mathbf{E}_1$.

2.1.1 Invariance to similarity transformations

Let $(\mathbf{x}_0, \mathbf{E}_0)$ and $(\mathbf{x}_1, \mathbf{E}_1)$ be a pair of oriented points whose rotational-flows interpolation is found by $f(t) = (\mathbf{x}_t, \mathbf{E}_t)$.

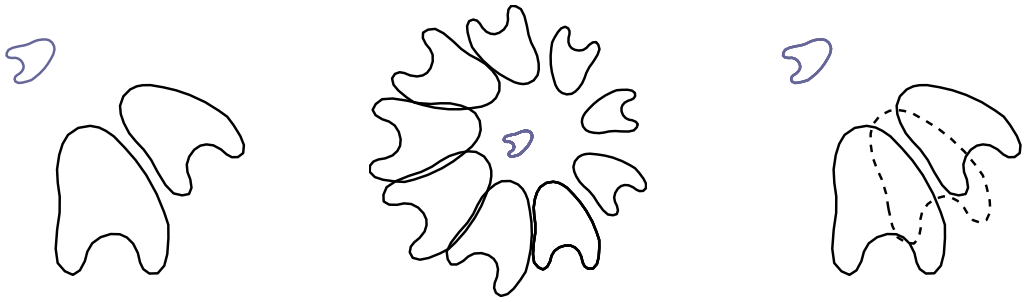

Figure 2. The centers of rotation implied by a pair of similar objects is itself similar to those objects. (Left) $S[0]$ and $S[1]$ (in black) and their center of rotation C (in purple). (Center) A set of curves (black) produced by rotating the points in $S[0]$ about the corresponding point in C (purple) . (Right) The interpolated curve $S[0.5]$ (dashed line) for this example.

Suppose that $\mathbf{R}$ defines a rotation, σ a uniform scaling and τ a translation. Let $g(\cdot)$ denote the rotational-flows interpolation from $(\sigma\mathbf{R}\mathbf{x}_0 + \tau, \mathbf{R}\mathbf{E}_0)$ to $(\sigma\mathbf{R}\mathbf{x}_1 + \tau, \mathbf{R}\mathbf{E}_1)$. It can be shown that

$$g(t) \quad = \quad (\sigma\mathbf{R}f(t) + \tau, \mathbf{R}\mathbf{E}_t) \tag{4}$$

2.1.2 Resumption of an interpolation

Let $f(\cdot)$ be the rotational-flows interpolation such that $f(0) = (\mathbf{x}_0, \mathbf{E}_0)$ and $f(1) = (\mathbf{x}_1, \mathbf{E}_1)$. For any $t : 0 < t < 1$ let $g_t(\cdot)$ be the rotational-flows interpolation between the interpolated oriented point $f(t)$ and $(\mathbf{x}_1, \mathbf{E}_1)$. It is a simple proof to show that $g_t(s) = f(t + s(1-t))$ and thus each interpolated point $g_t(s)$ lies on the path swept out by $f(\cdot)$. Note that $\mathbf{c}$ is equidistant to $\mathbf{x}_t$ and $\mathbf{x}_1$ so it lies on their perpendicular bisector. The angle $\angle(\mathbf{x}_t; \mathbf{c}; \mathbf{x}_1)$ is $(1-t)\cdot\theta$. This is precisely the amount of rotation needed to bring $\mathbf{E}_t$ to $\mathbf{E}_1$. This property is illustrated in the right pane of Fig. 1

2.1.3 Interpolation of a global similarity transformation

Suppose that the curve $S[0]$ is similar to $S[1]$. The local interpolations defined by (2) will produce interpolated objects $S[t]$ that are also similar to $S[0]$, as we will now demonstrate.

It is an easily proven consequence of (3), that if $S[1]$ can be produced by a similarity transformation of $S[0]$ that has no rotational component, the rotational-flows interpolation will interpolate that transformation such that every $S[t]$ is related to $S[0]$ by a similarity transformation of that form. The following theorems prove that this behavior also holds when $S[0]$ and $S[1]$ are related by a similarity transformation with a non-trivial rotation component.

Theorem 1 (Rotational centers for two similar sets) *Let $C = \{\mathbf{c}_i\}$ be the set of rotational centers defined in (1). Suppose that $S[1]$ can be produced by applying a similarity transform to $S[0]$ with the following components: rotation by an angle ϕ, uniform scaling by a factor σ, and translation by the vector $(\Delta x, \Delta y)$. C is similar to $S[0]$.*

Let i, j index two distinct points $\mathbf{x}_{i,0}$, $\mathbf{x}_{j,0}$ in $S[0]$ and their corresponding centers of rotation $\mathbf{c}_i$, $\mathbf{c}_j$.

$$\frac{\|\mathbf{c}_i - \mathbf{c}_j\|^2}{\|\mathbf{x}_{i,0} - \mathbf{x}_{j,0}\|^2} \quad = \quad \frac{(\sigma-1)^2}{4\left(\sin\frac{\phi}{2}\right)^2} \tag{5}$$

$$\angle(\mathbf{x}_i - \mathbf{x}_j; \mathbf{0}; \mathbf{c}_i - \mathbf{c}_j) \quad = \quad \frac{\pi + \phi}{2} \tag{6}$$

Let $\sigma' = (\sigma-1) / \left(2\sin\frac{\phi}{2}\right)$ and $\phi' = (\pi+\phi)/2$. When $\sigma > 1$, the formula for $\mathbf{c}_i$ is given in (7).

Substituting $\frac{1}{\sigma} \rightarrow \sigma$ into (5) and $-\phi \rightarrow \phi$ into (6), shows that the size and orientation of C are independent of which curve is given the name $S[0]$ and which is $S[1]$.

The left panel of Fig. 2 shows an example of a pair of similar shapes and the centers of rotation identified by our method. Here the curve $S[0]$ was taken from a manual contour of a bladder on its mid-axial slice in CT. $S[1]$ was produced by applying a known similarity transform to $S[0]$.

When $\phi = 0$, the denominator of (5) is 0. This is consistent with (3). Because there is no rotational component to our similarity transform, the method provides a straight-line interpolation which can be interpreted as rotation about points that are infinitely far away from the original data and from each other.

When $\sigma = 1$, (5) is 0 as C has collapsed into a single point that truly is the center for a rigid rotation. C is not strictly similar to $S[0]$ since there is no inverse transform which can recover the curve from the point in this case. However, collapsing to a point is the limiting behavior for similarity transforms as the scaling factor approaches 0.

$$\mathbf{c}_i = \sigma' \mathbf{R}_{\phi'} \mathbf{x}_{i,0} + \frac{1}{2}\left(\Delta x\,(\sigma+1) + \Delta y(\sigma-1)\cot\frac{\phi}{2}, \Delta y\,(\sigma+1) - \Delta x\left(\sigma-1\right)\cot\frac{\phi}{2}\right) \quad (7)$$

$$\frac{\|\mathbf{x}_{i,t} - \mathbf{x}_{j,t}\|^2}{\|\mathbf{x}_{i,0} - \mathbf{x}_{j,0}\|^2} = 1 + \frac{(\sigma-1)^2}{2\left(\sin\frac{\phi}{2}\right)^2} - \frac{\sigma-1}{\sin\frac{\phi}{2}}\left(\sin\left(\frac{\phi}{2} - t\phi\right) - \sin\left(\frac{\phi}{2}\right) + \frac{\sigma-1}{2\sin\frac{\phi}{2}}\left(\cos t\phi\right)\right) \quad (8)$$

Theorem 2 (Rotation about a similar set) *Let $\{\mu_\cdot\}$ denote a set of points in $\mathbb{R}^2$. Let $\{\nu_\cdot\}$ denote a set of similar points such that for each i, ν_i is formed by rotating μ_i by an angle of ϕ about the origin, scaling the result by σ, and then translating by $(\Delta x, \Delta y)$. Now let μ_i^ψ be found by rotating μ_i an angle of ψ about ν_i.*

$$\frac{\|\mu_i^\psi - \mu_j^\psi\|^2}{\|\mu_i - \mu_j\|^2} = 1 + 2\sigma^2 - 2\sigma\left(\cos\left(\phi\right) - \cos\left(\phi - \psi\right) + \sigma\cos\left(\psi\right)\right) \quad (9)$$

Equation (9) is a general statement: the new shape formed by rotating a shape about another similar shape, in the manner we have defined, is also similar to the original shape. When σ is 0, (9) simplifies to a well known truth: rotation about a single point is a rigid transformation.

The center pane of Fig. 2 shows the result of various rotations of a curve about a similar curve.

Theorem 3 (Rotational flows between similar objects) *Suppose again that $S\left[0\right]$ and $S\left[1\right]$ are related by a similarity transform with rotational component ϕ, scaling factor σ, and an arbitrary translational factor. Any $S\left[t\right]$ is similar to $S\left[0\right]$. The square of scaling factor from $S\left[0\right]$ to $S\left[t\right]$ is given by (8).*

Equation (8) follows from substituting (5, 6) into (9) and from (2) which states that $\angle\left(\mathbf{x}_{i,0}; \mathbf{c}_i; \mathbf{x}_{i,t}\right) = t\phi$. The rotational-flows interpolation between two similar curves is shape maintaining. An example of this property can be seen in the right pane of Fig. 2.

The special case of (8) when $\sigma = 1$ shows that the rotational-flows interpolation between two congruent curves is shape and size maintaining. When $\sigma > 1$, the derivative of (8) with respect to t is strictly positive over the interval $t \in [0, 1]$. Likewise, when $0 < \sigma < 1$, $\frac{d}{dt}$ (8) is strictly negative over that interval. Although (9) allows the set of points to collapse onto a single point, the monotonicity of scale when (8) is restricted to $t \in [0, 1]$ guarantees that the interpolation between similar, but non-trivial, shapes will not pass through the degenerate configuration.

2.2. Interpolation in three dimensions

Let $(\mathbf{x}_0, \mathbf{E}_0)$ and $(\mathbf{x}_1, \mathbf{E}_1)$ be corresponding oriented points in $\mathbb{R}^3$. There exists a unit vector $\mathbf{z}$ that defines the axis of rotation from $\mathbf{E}_0$ to $\mathbf{E}_1$. Let the magnitude of this rotation be denoted by $0 \leq \phi \leq \pi$. The three dimensional rotational-flows interpolation between these points is designed to rotate $\mathbf{x}_0$ by ϕ about the $\mathbf{z}$ axis as well.

Since $\mathbf{x}_0$ and $\mathbf{x}_1$ may lie in different planes that are normal to $\mathbf{z}$ we cannot assume that the desired rotational path between them exists. If we project $\mathbf{x}_0$ and $\mathbf{x}_1$ along $\mathbf{z}$ into a common plane, we can form a path that combines rotation about $\mathbf{z}$ with translation along $\mathbf{z}$. Let $z_0 = (\mathbf{x}_0 \cdot \mathbf{z})$ and $\mathbf{x'}_0 = \mathbf{x}_0 - z_0\mathbf{z}$. Let z_1 and $\mathbf{x'}_1$ be defined in a similar fashion. Let $f_2\left(t\right) = (\mathbf{x'}_t, \cdot)$ be the two-dimensional rotational-flows interpolation between these projected points. The three-dimensional rotational-flows interpolation is given by (10) and is illustrated in Fig. 3.

$$f\left(t\right) = \left(\mathbf{x'}_t + \left(z_0 + t\left(z_1 - z_0\right)\right)\mathbf{z}, \mathbf{R}_{\mathbf{z},t\phi}\mathbf{E}_0\right) \quad (10)$$

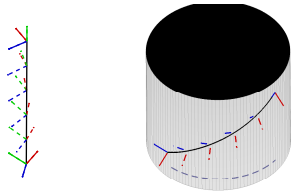

Figure 3. Three-dimensional rotational-flows interpolation. $\mathbf{x}_t$ lies on a helix whose axis is the axis of rotation between $\mathbf{E}_0$ and $\mathbf{E}_1$.

When the surfaces $S\left[0\right]$ and $S\left[1\right]$ are similar, the rotational-flows interpolation produces a transformation that is linear with respect to the vertex positions in homogeneous coordinates. The interpolated shapes are not necessarily similar to the end points since the scaling within the $\mathbf{z} = 0$ plane per (8) and the scaling due to the translation along the the $\mathbf{z}$ axis have different scale factors. In Section 3.2 we argue that rotational-flows interpolation is more shape preserving than a straight-line interpolation.

2.3. Interpolation of m-rep shape models

The discrete m-rep [10] provides a sampled medial representation for a shape in three dimensions. This representation has been used for a variety of applications in medical image analysis including shape modeling [7], image segmentation [9], and statistical shape analysis [6].

Each shape instance (referred to as an object or an m-rep for convenience) consists of a 2-D lattice of medial atoms

consisting of the following parameters: a position in the interior of the object, $\mathbf{x}(u,v)$, also known as a hub; a radius, $r(u,v)$ of an inscribed ball that is bitangent to the surface of the object and centered at the hub; and two spoke vectors $\mathbf{U}_{-1}(u,v)$ and $\mathbf{U}_{+1}(u,v)$. The inscribed ball intersects the object's boundary at $\mathbf{x}(u,v) + r(u,v)\,\mathbf{U}_{\pm 1}(u,v)$.

The medial atoms on the edges of the lattice have an additional (implied) spoke $\mathbf{U}_0(u,\ v)$ that is the unit vector in the direction of $(\mathbf{U}_{-1}(u,\ v)\ +\ \mathbf{U}_{+1}(u,\ v))$. and an additional scaling factor, $\eta(u,v)$ which is known as the elongation. The elongated implied spoke intersects the surface at $\mathbf{x}(u,v) + r(u,v)\,\eta(u,v)\,\mathbf{U}_0(u,v)$.

Fletcher [4] defined a metric on the space of medial atoms, but it measures changes in hub position independently from changes in spoke orientation. Consequently the geodesics under this metric are characterized by linear hub paths. Interpolation of medial atoms along such a geodesic produces a straight-line interpolation of the hubs.

We now describe rotational-flows interpolation between corresponding medial atoms (i.e., those with the same (u,v) coordinates) on different instances of the same shape. As a notational shortcut we will omit the (u,v) indices. We use the orientation of the medial axis at $\mathbf{x}$ to define the following frame that is used to interpolate the hubs using the method described in Section 2.2.

The $\mathbf{e}_1$ basis is chosen to be in the direction of $\mathbf{U}_{+1} - \mathbf{U}_{-1}$ because the difference between the spoke vectors is known to be normal to the medial axis. The $\mathbf{e}_2$ basis is in the direction of $\delta\mathbf{x}/\,\delta u - (\delta\mathbf{x}/\,\delta u \cdot \mathbf{e}_1)\,\mathbf{e}_1$. Because the directional derivative can only be estimated from the discretely sampled hub positions, it needs to be corrected to truly be tangent to the medial axis. The remaining basis is defined by $\mathbf{e}_3 = \mathbf{e}_1 \times \mathbf{e}_2$.

The radius and elongation of the m-rep are interpolated geometrically: $r_t = r_0\left(\frac{r_1}{r_0}\right)^t$ and $\eta_t = \eta_0\left(\frac{\eta_1}{\eta_0}\right)^t$. The spoke vectors are interpolated geodesically after accounting for rotation of the hubs. Let $\mathbf{U'}_{+1}$ represent the $\mathbf{U}_{+1}$ spoke in frame relative coordinates:

$\mathbf{U'}_{+1} = (\mathbf{U}_{+1}\cdot\mathbf{e}_1, \mathbf{U}_{+1}\cdot\mathbf{e}_2, \mathbf{U}_{+1}\cdot\mathbf{e}_3)^T$.

Let $\mathbf{U'}_{+1,0}$ and $\mathbf{U'}_{+1,1}$ represent those vectors at times 0 and 1 respectively. We define the axis $\mathbf{b}$ and angle ϕ as

$$\phi = \cos^{-1}(\mathbf{U'}_{+1,0}\cdot\mathbf{U'}_{+1,1}) \quad (11)$$

$$\mathbf{b} = (\mathbf{U'}_{+1,0}\times\mathbf{U'}_{+1,1}) \quad (12)$$

The spoke is interpolated geodesically in frame coordinates,

$$\mathbf{U'}_{+1,t} = \mathbf{R}_{\mathbf{b},t\phi}\mathbf{U'}_{+1,0} \quad (13)$$

$$\mathbf{U}_{+1,t} = \sum_{i=1}^{3}(\mathbf{U'}_{+1,t}\cdot\mathbf{e}_{i,t})\,\mathbf{e}_{i,t} \quad (14)$$

The other spoke, $\mathbf{U}_{-1}$ is interpolated in the same way. One desirable property of this interpolation is that it preserves the normality of the spoke difference to the medial sheet. This difference is collinear with $\mathbf{e}_1$, the direction normal to the interpolated medial axis.

3. Results

3.1. Interpolations of planar curves

Rotational-flows interpolations of planar curves are shown in Fig. 4. In each of these examples, $S[0]$ is drawn with the thinnest line. The line thickens at each time step with $S[1]$ drawn with the heaviest line.

The top row shows interpolations between pairs of similar ellipses. In pane 1, the reference and target curves are congruent. Their size and shape are maintained during the interpolation. In pane 2, the reference and target curves differ only in scale. None of the interpolated shapes have been rotated or translated. Pane 3 shows a full similarity transformation. Note that the centers of rotation are similar to the original and interpolated shapes. Pane 4 shows the interpolation between congruent ellipses after their correspondence has deliberately been corrupted. The interpolated shape are no longer ellipses.

The center row shows rotational-flows interpolation between shapes that are not similar. In panes 1 and 2, the interpolation is between two ellipses with different eccentricity. In the third pane the interpolation is between an ellipse and a bent curve. In these three sequences the interpolated curves are visually satisfying. Pane 4 shows an indentation forming during the interpolation between ellipses. It appears that this problem is related to poor correspondences between $S[0]$ and $S[1]$.

The bottom rows shows an interpolation where a concave region becomes convex. The curves $S[0]$ and $S[1]$ were formed by applying a bending transformation to an ellipse. Pane 1 is unsatisfactory because the interpolated shape $S[0.5]$ has two protrusions at each end: one from the downward bend and one from the upward bend. Pane 2 shows the rotational-flows interpolation using the standard ellipse as a key frame. This use of an intermediate key frame is a well known technique in the graphics literature. Another corrective technique from the graphics literature is to prealign shapes prior to the morph. In our experience, a translational alignment between shapes can lead to a more satisfying interpolation. In pane 3, the shapes have been prealigned and the interpolation is forced to pass through the standard ellipse. Our method is sensitive to the correspondences between the oriented points in $S[0]$ and $S[1]$. The fourth pane shows our interpolation on the original curves, after correspondences have been improved so that the curves are understood as rotated copies of each other.

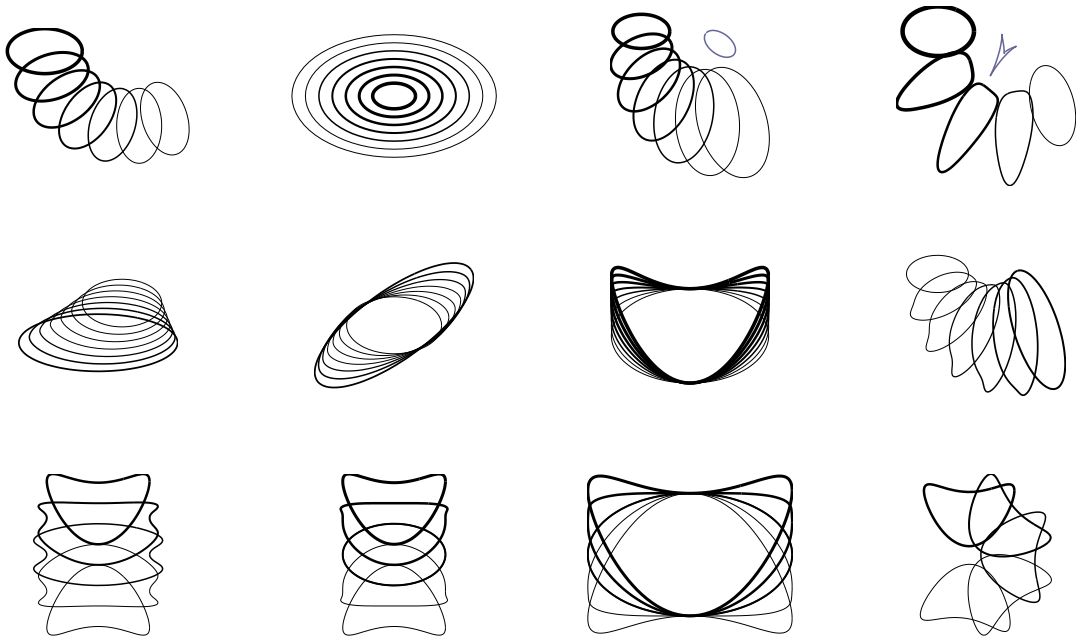

(1) (2) (3) (4)

Figure 4. Rotational-flows interpolation in two dimensions. In each example the time axis is denoted by line thickness. (Top) Interpolations between pairs of similar ellipses. (1) A rigid transformation. (2) Uniform scaling only. (3) A full similarity transformation. (4) A rigid transformation with poor correspondence between $S[0]$ and $S[1]$. (Center) Interpolation between non-similar curves. (1) Affine scaling and translation of the ellipse. (2) Affine scaling and rotation of the ellipse. (3) Bending of the ellipse. (4) A full affine transformation. In this case the interpolations deviate from the desired shape spaces of ellipses. (Bottom) Interpolation between shapes where a concave region becomes convex. (1) The original interpolation, note the pair of protrusions at each end of $S[0.5]$. (2) The interpolation has been forced to pass through an ellipse at $t = 0.5$. A single protrusion still exists at the ends of $S[0.25]$ and $S[0.75]$. (3) The shapes have been prealigned and $S[0.5]$ is forced to be the ellipse. Each $S[t]$ appears to be a bent version of the ellipse. (4) Correspondences have been redefined so that the interpolation is a shape-preserving rotation.

3.2. Shape preservation during three-dimensional interpolation

The top row of Fig. 5 shows the rotational-flows interpolation between two similar surfaces. As predicted, $S[0]$ is not similar to $S[t]$ for almost all $0 < t < 1$. However, we demonstrate that interpolated $S[t]$'s produced by rotational flows are more like $S[0]$ than the intermediate shapes produced by a linear interpolation.

Let $S[0]$ and $S[1]$ be similar shapes, and let $\mathbf{M}$ be the 4×4 matrix such that when the points in $S[0]$ and $S[1]$ are expressed in homogeneous coordinates, $S[1] = \mathbf{M}S[0]$. Let $\mathbf{M}_3$ denote the upper 3×3 block of $\mathbf{M}$. We use the fractional anisotropy (FA) [1] of $\mathbf{M}_3$, to measure the degree to which the transformation preserves shape. Let, $\lambda_1 \geq \lambda_2 \geq \lambda_3$ be the square roots of the eigenvalues of $\mathbf{M}_3\mathbf{M}_3{}^T$. Let $\bar{\lambda} = \frac{1}{3}\sum_{i=1}^{3} \lambda_i$. FA is defined as

$$fa(\lambda_1, \lambda_2, \lambda_3) = \sqrt{\frac{\frac{1}{2}\sum_i (\lambda_i - \bar{\lambda})^2}{\frac{1}{3}\sum_i \lambda_i^2}} \qquad (15)$$

The value of $fa(\cdot)$ ranges from 0 for a shape-preserving transformation to 1 for a transformation that collapses the shape onto a single axis.

Using $S[0]$ and $S[1]]$ as defined in the top row of Fig. 5, we compared the fractional anisotropy of the transformation from $S[0]$ to $S[t]$ for straight-line and rotational-flows interpolations. The left pane of Fig. 6 shows that the rotational-flows interpolation between similar shapes is more shape preserving than straight-line interpolation.

To further understand the performance of rotational-flows interpolation versus straight-line interpolation, we ran the following experiments. We took the known similarity transformation that took $S[0]$ to $S[1]$ in the previous example, and generated new target surfaces, $S_\phi[1]$ by setting the angle of rotation in the transformation to be ϕ while holding the other parameters constant. For each ϕ we measured the maximum fractional anisotropy of the transformation from $S[0]$ to $S_\phi[t]$ over $t \in [0, 1]$ for rotational-flows and straight-line interpolations. We performed a similar experiment varying the scale parameter of the similarity transfor-

mation while holding the rotation and translation constant. The results of these experiments are plotted in the central panes of Fig. 6.

In both experiments, the rotational-flows interpolation was more shape preserving than straight-line interpolations. Moreover, the level of fractional anisotropy was quite low for all scales we considered and for the majority of rotation angles we explored. However, as the angle of rotation approached 180 degrees, our method lost its ability to maintain the shape of the interpolated objects.

In the general case, when $S[0]$ and $S[1]$ are not similar, the three-dimensional rotational-flows interpolation frequently produces intermediate shapes that appear reasonable. An example of such is shown in the bottom row of Fig. 5. Although there is no linear transformation from $S[0]$ to $S[t]$ in this example, the fractional anisotropy of the least squares estimates of such a transformation is a monotonic function with maximum at $t = 1$. As shown in the right pane of 6, this compares favorably with interpolation by linear paths. In that case, there is a spurious maximum of fractional anisotropy for an interpolated shape.

3.3. An example using m-reps

We fit m-rep models to a time series of lung segmentations using the method of Han *et al*. [7]. Figure 7 shows the rotational-flows interpolation from our model at peak inspiration to our model at peak expiration. Informally, our interpolated surfaces exhibit the behavior we expect from a lung during exhalation. The lung is decreasing in volume, and the most visible motion is where the inferior portion rises away from the diaphragm.

4. Discussion

We have proposed a novel method for shape interpolation that moves oriented points along easily computed and understood rotational paths that combine changes in position and orientation. This interpolation offers superior shape maintenance when compared with the linear interpolation of the points without regard for changes in orientation. We have demonstrated our method with interpolations of synthetic data sets in two and three dimensions and with interpolations of medial shape models derived from patient data.

Our method cannot guarantee that it will produce diffeomorphic transformations. Our future work includes developing a better understanding of conditions on our target and reference objects that lead to two interpolated points occupying the same position at some intermediate time. Similarly we need to develop a method to automatically modify the interpolation to overcome such a failure. Once we have these failures and their recovery is better understood, we will be able to explore extrapolating the paths from our interpolation to deform an entire image volume.

A second line of future work that we plan to pursue is using this interpolation scheme to define a metric on shapes. Initially such a metric would be used for alignment and computation of a Fréchet mean shape. Further work is needed to compute higher order statistics using this metric.

References

[1] P. J. Basser and C. Pierpaoli. Microstructural and physiological features of tissues elucidated by quantitative-diffusion-tensor mri. *Journal of Magnetic Resonance, Series B*, 111:209–219, 1996. 6

[2] D. Breen and R. Whitaker. A level-set approach for the metamorphosis of solid models. *Visualization and Computer Graphics, IEEE Transactions on*, 7(2):173–192, Apr-Jun 2001. 1

[3] I. Chavel. *Riemannian Geometry: A Modern Introduction*. Cambridge University Press, 2006. 1

[4] P. T. Fletcher, C. Lu, S. M. Pizer, and S. Joshi. Principal geodesic analysis for the study of nonlinear statistics of shape. *Medical Imaging, IEEE Transactions on*, 23:995–1005, 2004. 1, 5

[5] J. Glaunes and S. Joshi. Template estimation form unlabeled point set data and surfaces for computational anatomy. In X. Pennec and S. Joshi, editors, *Mathematical Foundations of Computational Anatomy: Geometrical and Statistical Methods for Modelling Biological Shape Variability*, pages 58–65, October 2006. 1

[6] K. Gorczowski, M. Styner, J.-Y. Jeong, J. Marron, J. Piven, H. Hazlett, S. Pizer, and G. Gerig. Statistical shape analysis of multi-object complexes. *Computer Vision and Pattern Recognition, 2007. CVPR '07. IEEE Conference on*, pages 1–8, 17-22 June 2007. 4

[7] Q. Han, D. Merck, J. Levy, C. Villarruel, J. Damon, E. Chaney, and S. Pizer. Geometrically proper models in statistical training. In *Proceedings of Information Processing in Medical Imaging*, pages 751–762, 2007. 4, 7

[8] S. Joshi and M. Miller. Landmark matching via large deformation diffeomorphisms. *Image Processing, IEEE Transactions on*, 9(8):1357–1370, Aug 2000. 1

[9] S. Pizer, P. Fletcher, S. Joshi, A. Gash, J. Stough, A. Thall, G. Tracton, and E. Chaney. A method & software for segmentation of anatomic object ensembles by deformable m-reps. *Medical Physics*, 32(5):1335–1345, May 2005. 4

[10] S. Pizer, T. Fletcher, Y. Fridman, D. Fritsch, A. Gash, J. Glotzer, S. Joshi, A. Thall, G. Tracton, P. Yushkevich, and E. Chaney. Deformable m-reps for 3d medical image segmentation. *International Journal of Computer Vision*, 55(2):85–106, November-December 2003. 1, 4

[11] M. Vaillant and J. Glaunes. Surface Matching via Currents. *Proceedings of Information Processing in Medical Imaging (IPMI 2005)*, pages 381–392, 2005. 1

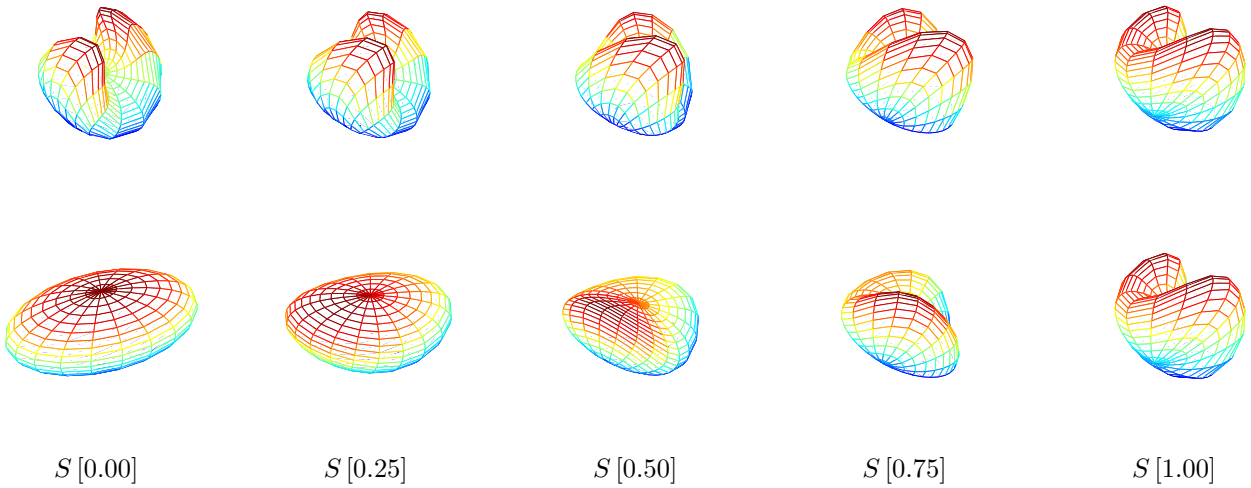

$S\,[0.00]$ $S\,[0.25]$ $S\,[0.50]$ $S\,[0.75]$ $S\,[1.00]$

Figure 5. Rotational-flows interpolation in three dimensions. (Top) between similar shapes. (Bottom) between non-similar shapes.

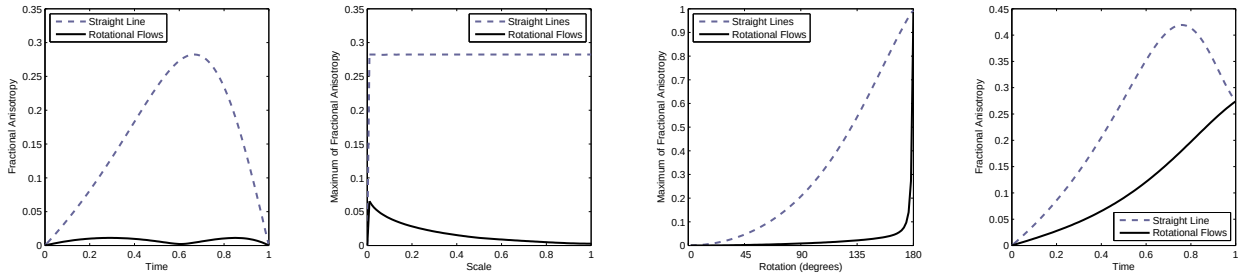

Figure 6. Comparing fractional anisotropy for transformations produced by rotational flows with those produced by straight-line interpolation. (Left) FA of the linear transformation from $S\,[0]$ to $S\,[1]$ for the top example of Fig. 5. (Inner-Left) As scale varies, $\max_{0<t<1}$ FA of the transformation from $S\,[0]$ to $S\,[t]$. (Inner-Right) As angle of rotation varies, $\max_{0<t<1}$ FA of the transformation from $S\,[0]$ to $S\,[t]$. (Right) FA of the linear approximation of the transformation from $S\,[0]$ to $S\,[1]$ for the example in the bottom row of Fig. 5.

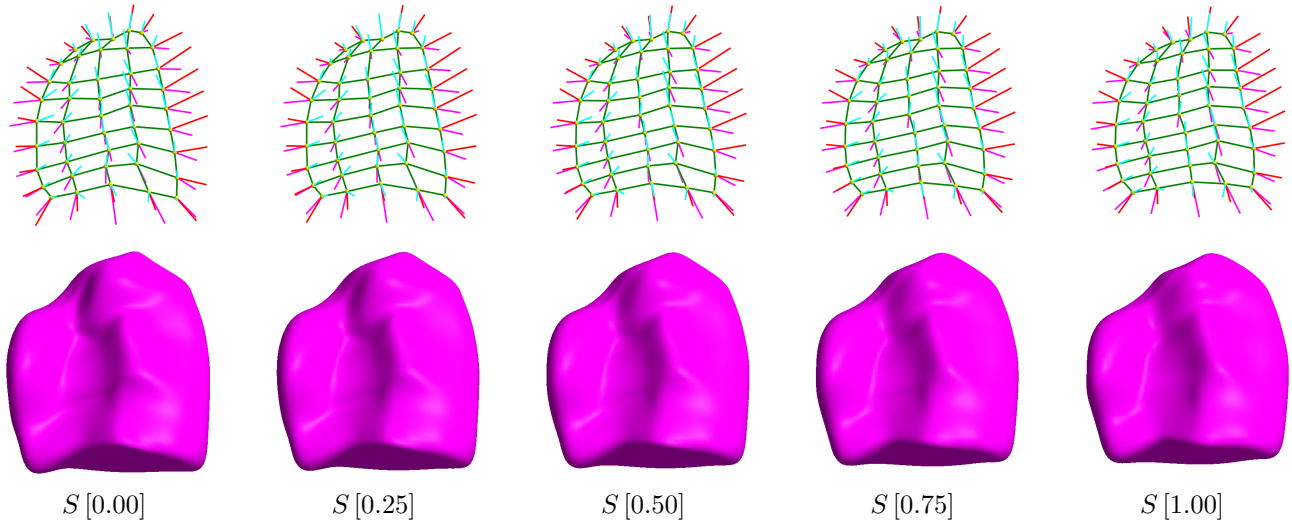

$S\,[0.00]$ $S\,[0.25]$ $S\,[0.50]$ $S\,[0.75]$ $S\,[1.00]$

Figure 7. Rotational-flows interpolation of m-rep lung models. $S\,[0]$ corresponds with peak inspiration. $S\,[1]$ corresponds with peak expiration. (Top) The m-rep object. (Bottom) The implied surface boundary.